New principles of design and operation for HVDC grids

Aleksandra Lekić

April 2021

Contents

Nomenclature

Constants and functions

$\widehat{f}$ averaged signal f over switching frequency

Parameters

f, ω line frequency and angular frequency

v_j phase $j \in \{a, b, c\}$ to neutral voltage

i_j phase current $j \in \{a, b, c\}$

v_{dc} DC voltage

i_{dc} DC current, assumed as constant and equal $i_{dc} = I_{dc}$

1   Power Electronic Converters

Integration of Renewable Energy Sources (RES) into electrical power system requires extensive application of power electronic converters. Commonly used power electronic converters are Line Commutated Converters (LCCs) and Voltage Source Converters (VSCs).

1.1   Line-Commutated Converter

Line-commutated converters (LCCs) are state-of-the-art since seventies. In Fig. 1 is depicted 12-pulse LCC for Pole 2 of the HVDC Inter-Island between the North and South Islands of New Zealand.
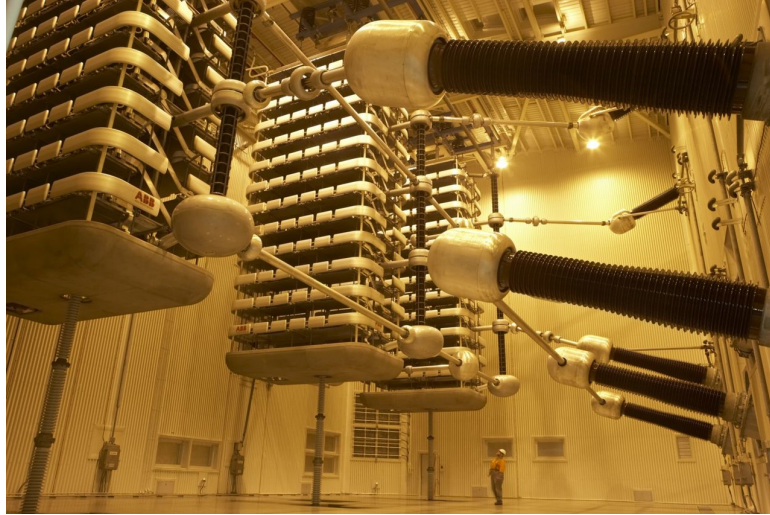

Figure 1: Thyristor valve, picture taken from wikipedia.

Line-Commutated Converter is designed using thyristors as switches, as depicted in Fig. 2 [1]. In Fig. 2 is depicted 6-pulse Graetz bridge [2, 3]. Thyristors are turned on α radians after the corresponding line-to-neutral voltage becomes maximal/minimal. Angle α is also called a firing angle.
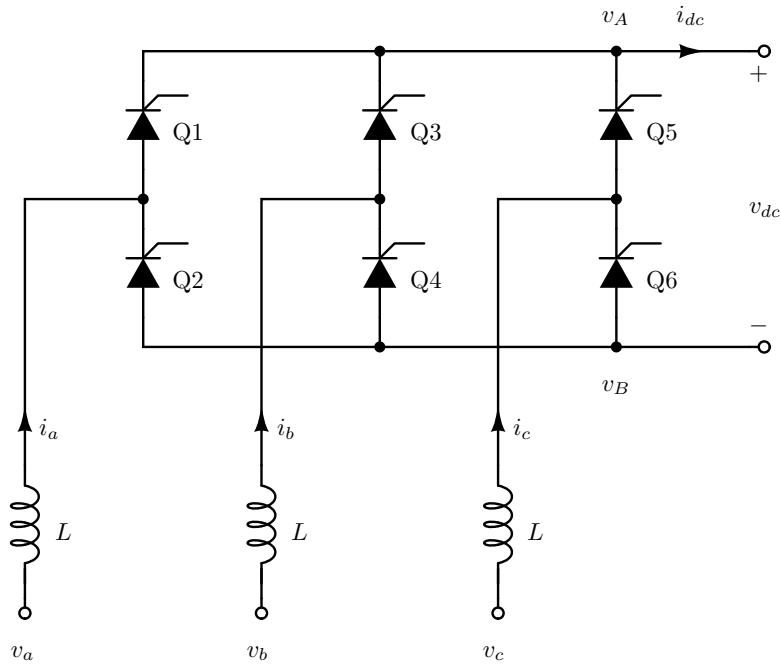

Figure 2: Line-commutated converter.

Let us first conduct the analysis considering that the inductors have infinite values, $L \rightarrow \infty$. When we consider $L \rightarrow \infty$, then the inductor represents the short connection. This case presents ideal commutation [4]. During whole analysis, we will consider thyristors as ideal switches, i.e. short connection while conducting and

open connection when they do not conduct. In that case, the expected waveforms are given in Fig. 3, where:

$$v_A(\omega t) = v_j(\omega t) \qquad \text{for } j = \arg\max(v_1(\omega t - \alpha), v_2(\omega t - \alpha), v_3(\omega t - \alpha)), \tag{1a}$$

$$v_B(\omega t) = v_j(\omega t) \qquad \text{for } j = \arg\min(v_1(\omega t - \alpha), v_2(\omega t - \alpha), v_3(\omega t - \alpha)), \tag{1b}$$

$$v_d(\omega t) = v_A(\omega t) - v_B(\omega t), \tag{1c}$$

$$i_j(\omega t) = \begin{cases} I_{dc} & \text{when } Q_{2j-1} \text{ is turned on,} \\ -I_{dc} & \text{when } Q_{2j} \text{ is turned on,} \\ 0 & \text{otherwise,} \end{cases} \tag{1d}$$

$$i_{dc}(\omega t) = I_{dc}. \tag{1e}$$

In the simulated case (Fig. 3) is taken that $\alpha = \frac{\pi}{6}$. Similarly can be obtained diagrams for different values for α.

For this case, the DC voltage can be calculated as

$$V_d = \frac{6}{\omega T} \int\limits_{\alpha}^{\alpha + \frac{\pi}{3}} v_{ac}(\omega t) d(\omega t),$$

and the expression is

$$V_d = \frac{3\sqrt{3}V_m}{\pi} \cos\alpha. \tag{2}$$

The estimated output power is

$$P = \frac{3\sqrt{3}I_{dc}V_m}{\pi} \cos\alpha. \tag{3}$$

In this case power factor is

$$PF = \frac{3}{\pi} \cos\alpha. \tag{4}$$

When L has some finite value, then we have commutation between thyristors. That means that when one thyristor turns on, the one that was already turned cannot right away turn off.

Let us observe commutation between thyristors Q1 and Q3 when $\omega t = \frac{\pi}{2}$. Both thyristors are turned on until current of Q3 reaches value of the DC current I_{dc}. This moment can be estimated from the following equations:

$$i_a + i_b = I_{dc}, \tag{5a}$$

$$v_a - L\frac{di_a}{dt} = v_b - L\frac{di_b}{dt}, \tag{5b}$$

which knowing that $\frac{di_a}{dt} = -\frac{di_b}{dt}$, forms differential equation

$$\frac{di_b}{dt} = \frac{v_b - v_a}{2L} = \frac{V_m\sqrt{3}}{2L} \sin\left(\omega t - \frac{\pi}{3}\right). \tag{6}$$

By integrating it in the limits $\frac{\pi}{3} + \alpha$ and $\frac{\pi}{3} + \alpha + \mu$, we get an expression for current i_b:

$$i_b(\omega t) = \frac{V_m\sqrt{3}}{2\omega L} (\cos(\alpha) - \cos(\alpha + \mu)). \tag{7}$$

Finally, the moment when all current is translated into thyristor Q3 is given with:

$$\mu = \arccos\left(\cos(\alpha) - \frac{2\omega L I_{dc}}{V_m\sqrt{3}}\right) - \alpha. \tag{8}$$

During mentioned commutation, voltage at the point A is $v_A = \frac{v_1 + v_2}{2}$.

Waveforms now become as depicted in Fig. 4. Values used for the simulation are given in table 1. Using the previous calculation, we can estimate DC voltage and power factor as [3]:

$$V_d = \frac{3\sqrt{3}V_m}{\pi} \cos\alpha - \frac{3\omega L I_{dc}}{\pi}, \tag{9a}$$

$$PF = \frac{2V_d I_{dc}}{V_m I_m}, \tag{9b}$$

where $I_m = \frac{2\sqrt{3}I_{dc}}{\pi} \frac{\sin(\mu/2)}{\mu/2}$ represents the first harmonic of the AC current.

It should be noted that if the firing angle α is greater than $\frac{\pi}{2}$, the output DC voltage is negative.
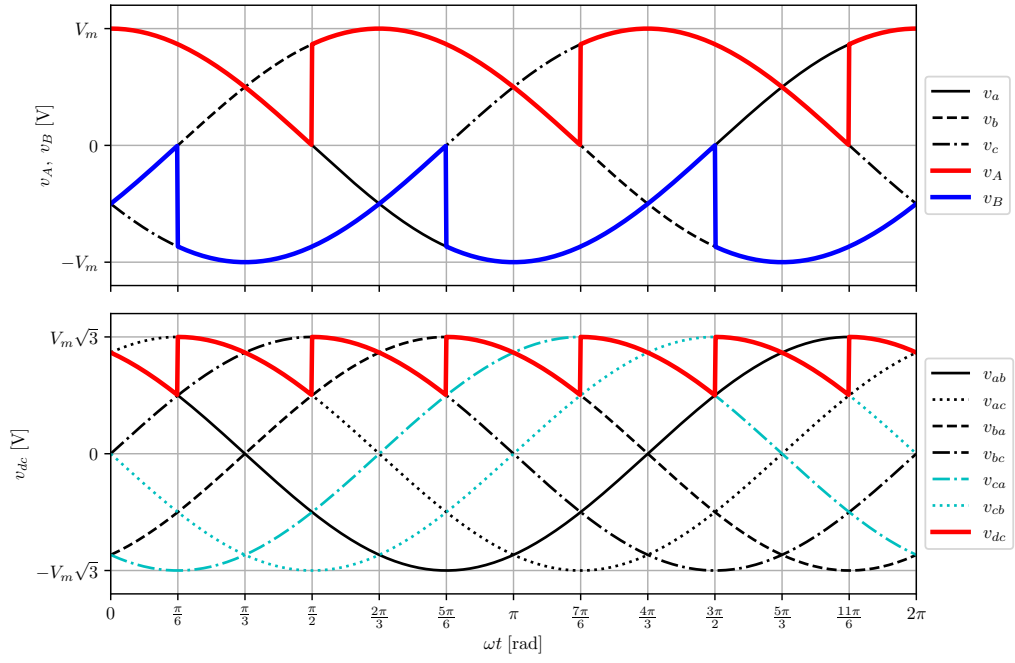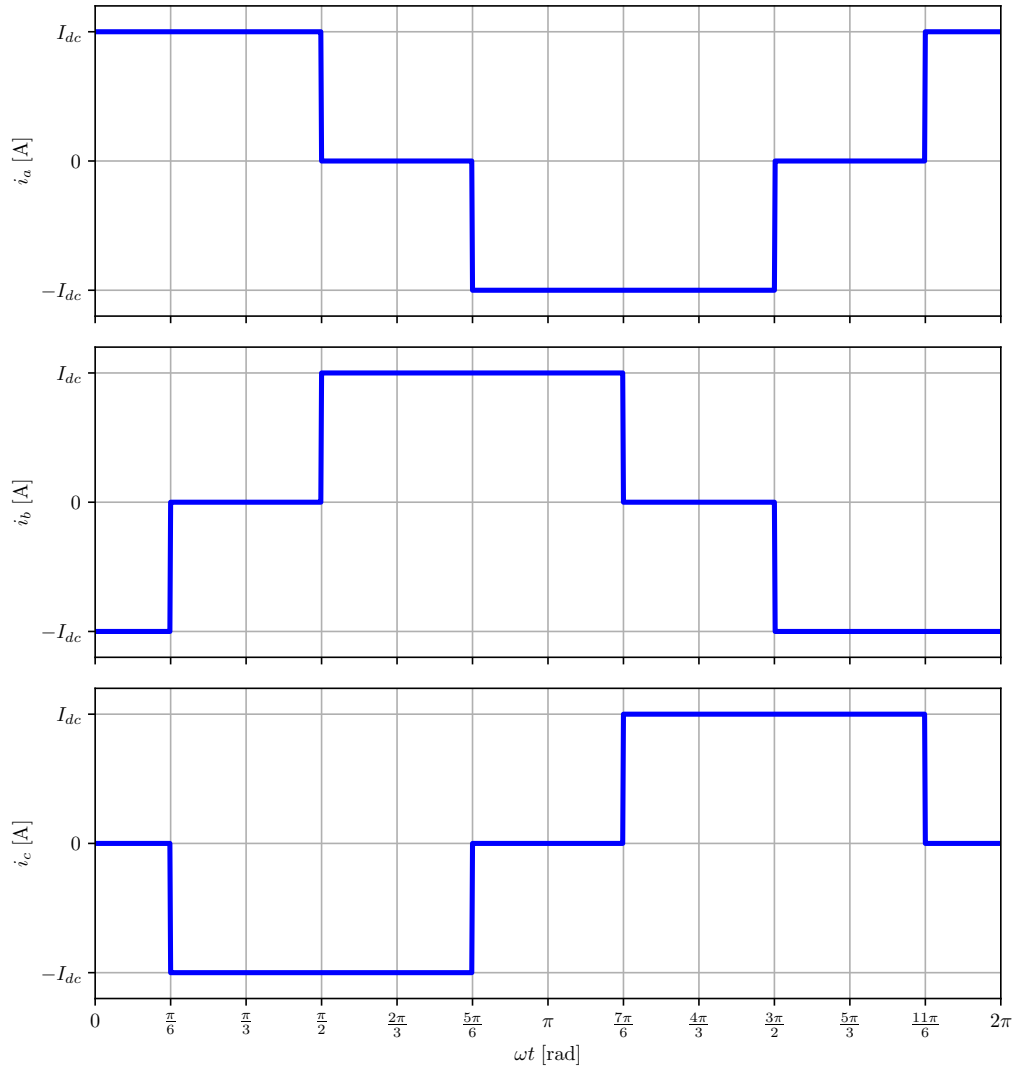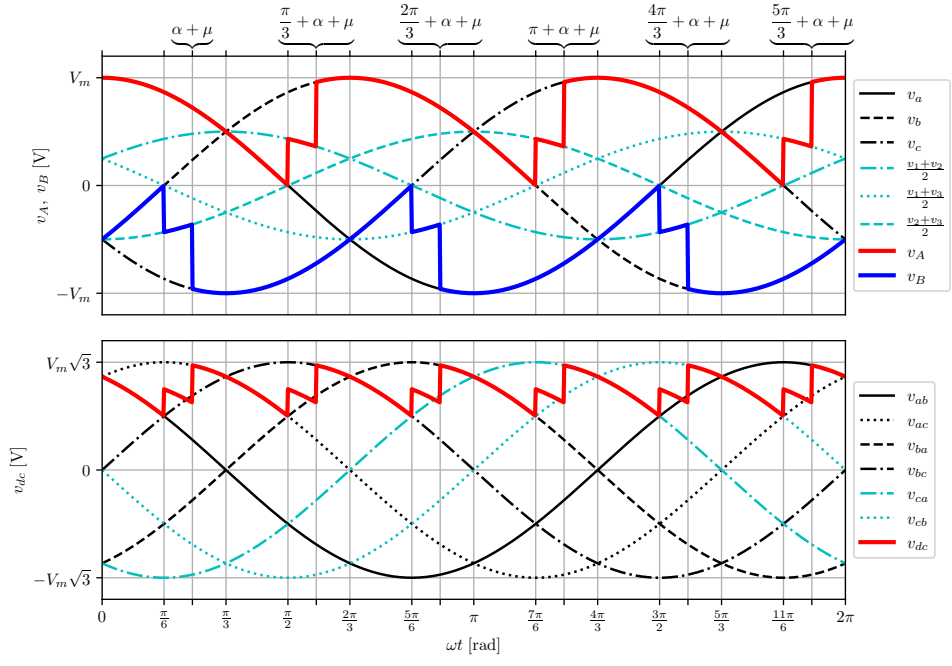
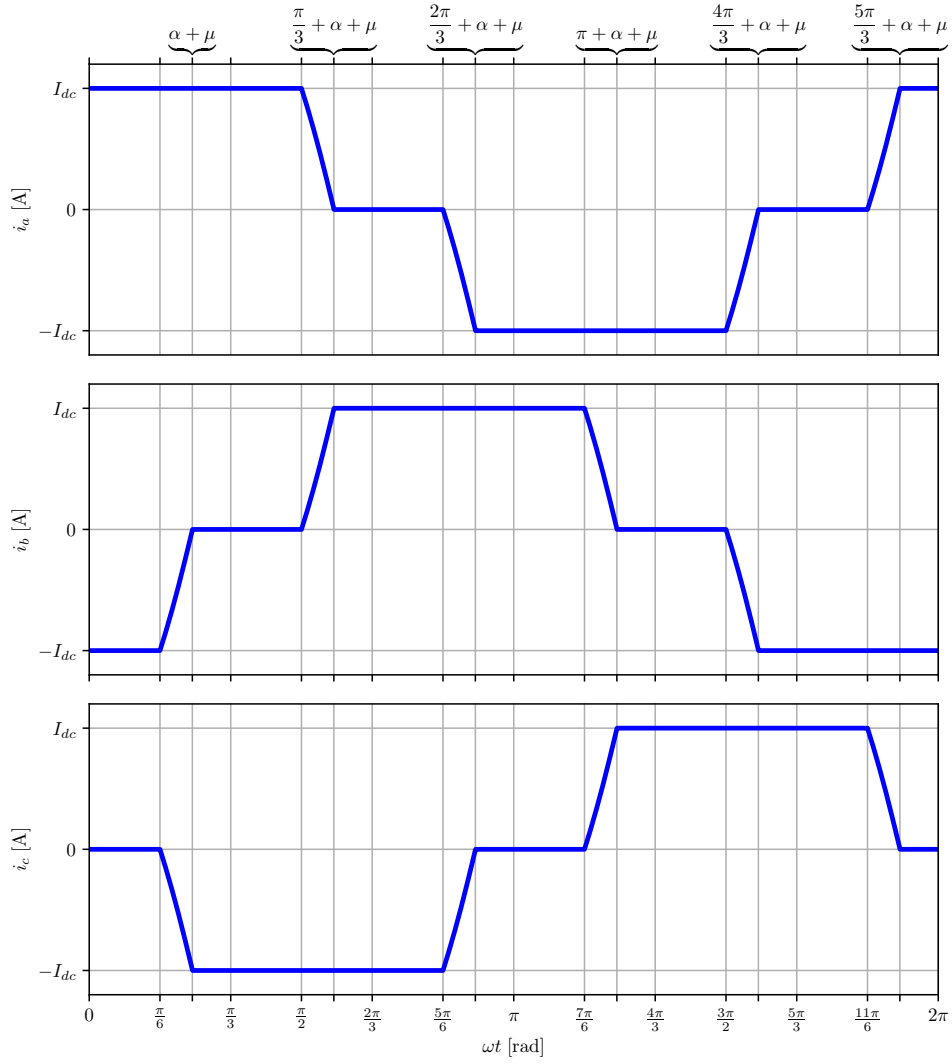Figure 3: Waveforms of the LCC with assumtion of $L \to \infty$ for (a) voltages, and (b) currents.

Figure 4: Waveforms of the LCC with assumption of finite value for L for (a) voltages, and (b) currents.

Table 1: Parameters of the 6-pulse LCC

f	50 Hz		V_{dc}	500 kV
I_{dc}	2 kA		V_m	345 kV
L	68.2 mH		α	$\frac{\pi}{6}$

1.1.1 Control Design

For the LCC the control is designed using control layers [4]. It consists of voltage dependent current order limit (VDCOL), a current controller (CC), an extinction angle controller (γ controller), phase locked loop (PLL), and firing pulse generator.

Voltage Dependent Current Order Limit (VDCOL): It is considered undesirable to have rated DC current flowing in the system whilst in an under-voltage situation. Hence, the DC voltage is taped by the VDCOL control circuit as shown in Fig. 5, where it is filtered by a first-order delay block. Using this filtered voltage in a look-up table, the lowest permissible voltage limit and the corresponding maximum permissible current I_{ref} is extracted [3]. This I_{ref} is used as a reference for the current controller.
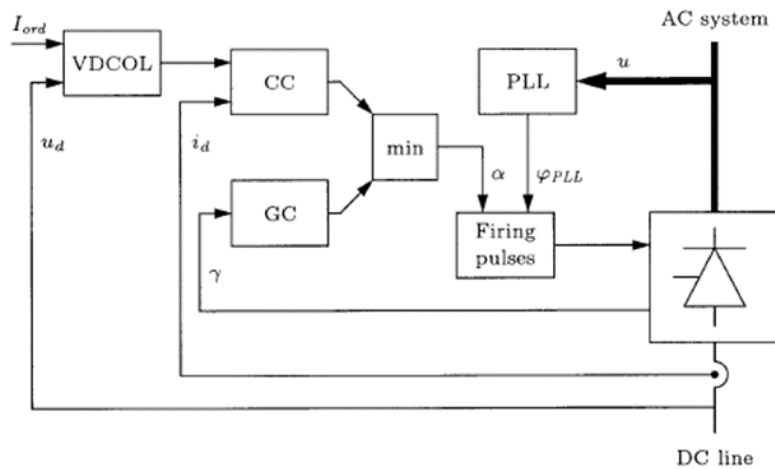

Figure 5: Classical implementation of LCC controls, picture taken from [3].

Current Controller is the real-time dc current is passed through a first-order delay block for filtering and then summed with some supplementary or reference signals obtained from the VDCOL layer [5]. The resultant signal is then passed to a PI controller so as to obtain the firing angle order. The obtained firing angle order is then limited by a limit block with predefined fixed limits obtained from other layers.

Gamma Controller: For an LCC inverter operating in an HVDC system, it must be ensured that the commutation process from one set of valves to the other must take place before the voltage of the extinguishing valve is positive again. This is ensured through a gamma controller as shown in Fig. 5. The commutation margin γ or "the time delay between the extinction of the valve and the valve voltage becoming positive again" is added to a negative fixed set-point (minimum commutation margin). The resultant difference is filtered through a limit block and then passed to a PI controller. The PI controller is designed in such a way that it saturates at the maximum firing angle order limit if the gamma value is higher than required. If not, the γ value is corrected to the minimal set-point. This, together with the current controller, helps in setting the firing angle order for an LCC inverter.

Phase Locked Loop (PLL): Any firing pulse generator requires a reference signal which is in synchronous with the system voltage. To obtain such a reference signal, especially in weak AC systems, a PLL (usually based on the space-vector concept) is required. As shown in Fig. 5, the PLL takes the system voltages as input in the abc domain and converts it into the space vector domain. This is done to simplify the mathematical integration of the power system and the control system by keeping the analytical equations independent of time. This can be achieved by performing Clark transformation on the abc domain parameters so as to obtain a complex rotating phasor. Subsequently, this rotating phasor can be made non-rotating by applying a bidimensional rotation transformation, which further simplifies the parameters mathematically.

1.2 Voltage Source Converter

Voltage source converter (VSC) is another class of HVDC-based power electronic converters, which are designed using IGBTs as switches. There are few classes of widely used VSCs: two-level, three-level converters, and modular multilevel converters.

In the following text two-level converter and MMC will be analyzed in detail.

1.2.1 Two-level Converter

In Fig. 6 is depicted two-level converter. Switches in the same arm are operated complementary, e.g. $Q3 = \overline{Q1}$. In Fig. 7 is depicted one arm operation, where is visible that when Q1 is conducting $v_{c,a} = \frac{v_{dc}}{2}$, and when Q3 conducts $v_{c,a} = -\frac{v_{dc}}{2}$. VSC can have square-mode operation, where each switch (IGBT) conducts for a half
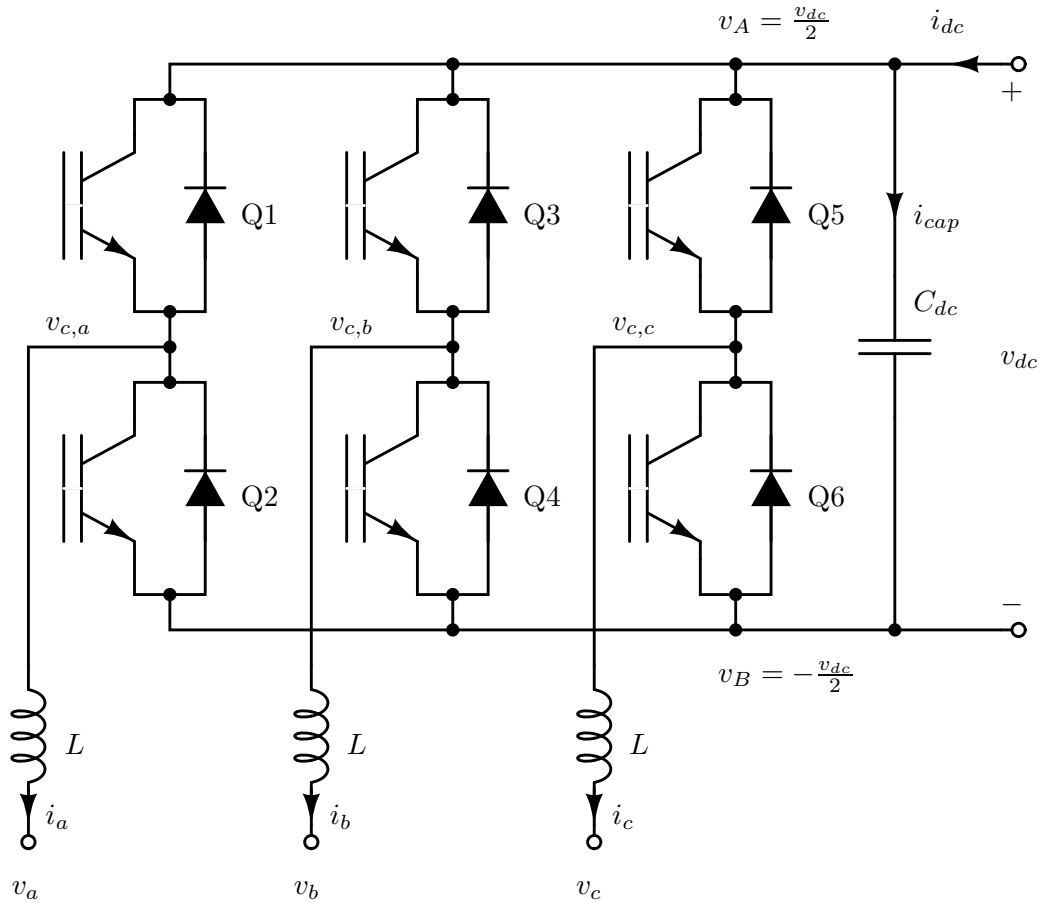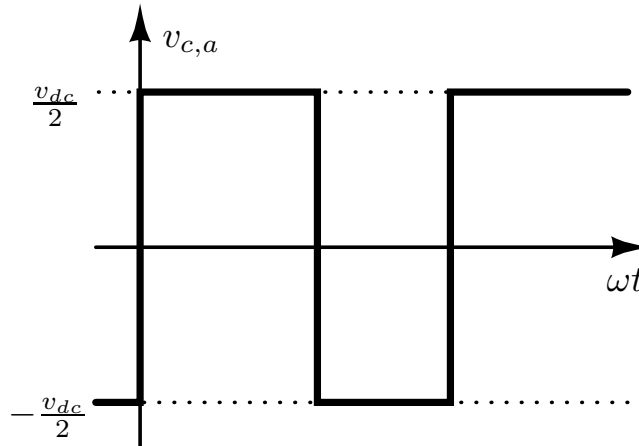

Figure 6: Two-level VSC.

Figure 7: One arm operation of the VSC.

period, with the phase shift of $\frac{2\pi}{3}$ for each phase [5]. This modulation is no longer used because it cannot vary

8

magnitude.

Therefore, VSCs are usually controlled using Pulse Width Modulation (PWM). PWM can be design on various ways, but the goal for it is to ensure that the averaged (over converter's switching frequency) currents and voltages have the desired waveforms (usually sine waveforms).

1.2.1.1 Averaged model

PWM modulated two-level VSC should have desired voltage/current waveforms. Therefore, for the further analysis is introduced dimensionless parameter denoted as modulation index and represented as m_j for $j \in \{a, b, c\}$ being the phase. For the each switching interval $m_j(t) \in [0, 1]$.

The converter operates in such manner that in the steady-state is $v_A = \frac{v_{dc}}{2}$ and $v_B = -\frac{v_{dc}}{2}$. The following equations can be written

$$\widehat{v_{C,j}} = \widehat{m_j}\frac{v_{dc}}{2}, \tag{10a}$$

$$L\frac{d\widehat{i_j}}{dt} = v_j - \widehat{v_{C,j}}, \tag{10b}$$

$$C_{dc}\frac{d\widehat{v_{dc}}}{dt} = \widehat{i_{cap}}. \tag{10c}$$

In addition we can write energy-balance equation as:

$$\widehat{v_{dc}}\left(\widehat{i_{dc}} - \widehat{i_{cap}}\right) = \sum_{j\in\{a,b,c\}} \widehat{v_{C,j}}\,\widehat{i_j},$$

which gives connection

$$\widehat{i_{cap}} = \widehat{i_{dc}} - \frac{1}{2}\sum_{j\in\{a,b,c\}} \widehat{m_j}\,\widehat{i_j}.$$

Finally, the complete set of differential equations with neglected variations on DC voltage is

$$v_{C,j} = m_j\frac{v_{dc}}{2}, \tag{11a}$$

$$L\frac{di_j}{dt} = v_j - v_{C,j}. \tag{11b}$$

Averaged notation is not used in the previous equations (11) due to simplicity of description.

1.2.2 Modular Multilevel Converter

MMC physical appearance is presented in Fig. 8. In Fig. 9 is depicted one arm of an MMC. With SMs are denoted submodules which can be: half-bridge (HB), full-bridge (FB), flying-capacitor, cascaded half-bridge, and double clamp [6]. However, HB and FB are usually used.

HB submodule is depicted in Fig. 10, where is visible that it has two operation modes. Switches have complementary operation, and SM can be conducting (when upper switch S1 conducts) or blocking (when $\overline{S1}$ conducts). The averaged output voltage is $\widetilde{v_H} = S_1 v_C$.

FB submodule is depicted in Fig. 11. It has three operation modes: when S1 and $\overline{S2}$ conduct – voltage $v_H = v_C$, S1 and S2 (or $\overline{S1}$ and $\overline{S2}$) conduct – $v_H = 0$, and when $\overline{S1}$ and S2 conduct – $v_H = -v_c$. The averaged voltage at the output is then $\widetilde{v_H} = (S_1\overline{S_2} - \overline{S_1}S_2)v_C$.

1.2.2.1 Averaged model

The converter topology is depicted in Fig. 9, for a single phase of a three-phase MMC. Variables from the Fig. 9 are defined for all three phases, $j \in \{a, b, c\}$. Submodules are considered with their averaged equivalents, and thus, the following equations for voltage and current can be written for the upper and lower arms:

$$v_{Mj}^{U,L} = m_j^{U,L}v_{Cj}^{U,L}, \qquad i_{Mj}^{U,L} = m_j^{U,L}i_j^{U,L}, \tag{12}$$

where $m_j^{U,L}$ are the corresponding upper and lower arm insertion indices, and $v_{Cj}^{U,L}$ is upper and lower are submodules' capacitor voltage.

The converter model is developed by following the $\Sigma - \Delta$ nomenclature, the variables in the upper and lower converter arms can be represented as:

$$i_j^\Delta = i_j^U - i_j^L, \quad i_j^\Sigma = \frac{i_j^U + i_j^L}{2},$$
$$v_{Cj}^\Delta = \frac{v_{Cj}^U - v_{Cj}^L}{2}, \quad v_{Cj}^\Sigma = \frac{v_{Cj}^U + v_{Cj}^L}{2},$$
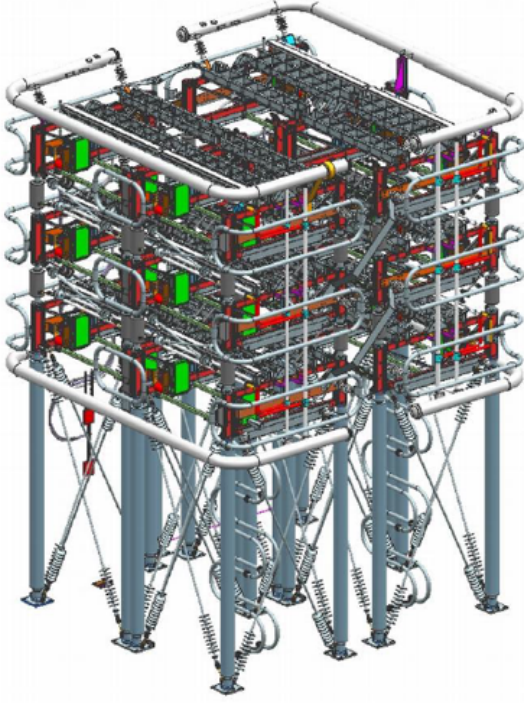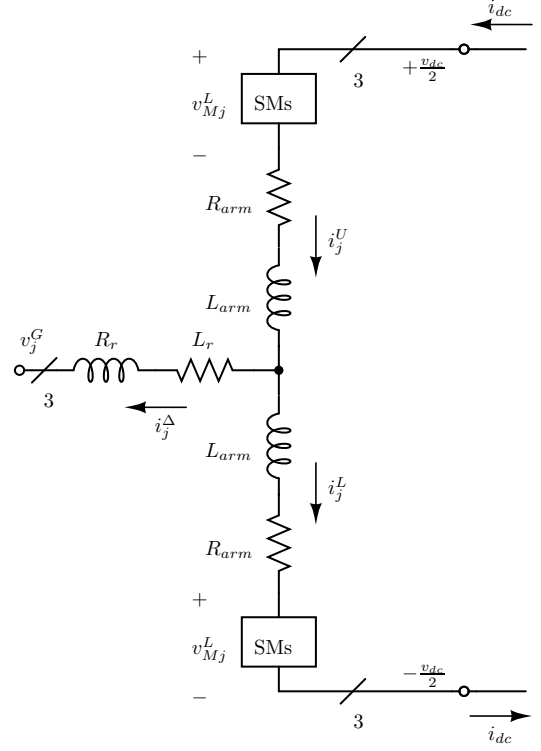
Figure 8: MMC picture.

Figure 9: MMC model.

$$
\begin{aligned}
m_j^\Delta &= m_j^U - m_j^L, \quad m_j^\Sigma = m_j^U + m_j^L, \\
v_{Mj}^\Delta &= \frac{-v_{Mj}^U + v_{Mj}^L}{2} = -\frac{m_j^\Delta v_{Cj}^\Sigma + m_j^\Sigma v_{Cj}^\Delta}{2}, \\
v_{Mj}^\Sigma &= \frac{v_{Mj}^U + v_{Mj}^L}{2} = \frac{m_j^\Sigma v_{Cj}^\Sigma + m_j^\Delta v_{Cj}^\Delta}{2}.
\end{aligned}
$$

With the new variables that have Σ and Δ superscripts, the equations of the state variables can be derived. In order to obtain the equations in multiple dqz frames, Park's transformation given in (21) is used with different frequencies.

The parameters are $L_{eq}^{ac} = L_r + \frac{L_{arm}}{2}$, $R_{eq}^{ac} = R_r + \frac{R_{arm}}{2}$, and C represents the submodule capacitor value and N the number of submodules in one converter arm. An equivalent DC-side capacitance $C_{dc} = 6\frac{C}{N}$ is used to model the DC voltage as a state variable. Taking into account previous writing convention, the following equations can be derived:

$$
v_{Mj}^\Delta = -\frac{m_j^\Delta v_{Cj}^\Sigma + m_j^\Sigma v_{Cj}^\Delta}{2}, \tag{13a}
$$

$$
v_{Mj}^\Sigma = \frac{m_j^\Sigma v_{Cj}^\Sigma + m_j^\Delta v_{Cj}^\Delta}{2}, \tag{13b}
$$

and differential equations:

$$
L_{eq}^{ac} \frac{di_j^\Delta}{dt} = v_{Mj}^\Delta - v_j^G - R_{eq}^{ac} i_j^\Delta, \tag{14a}
$$

$$
L_{arm} \frac{di_j^\Sigma}{dt} = \frac{v_{dc}}{2} - v_{Mj}^\Sigma - R_{arm} i_j^\Sigma, \tag{14b}
$$

$$
2C_{arm} \frac{v_{Cj}^\Delta}{dt} = m_j^\Sigma \frac{i_j^\Delta}{2} + m_j^\Delta i_j^\Sigma, \tag{14c}
$$

$$
2C_{arm} \frac{dv_{Cj}^\Sigma}{dt} = m_j^\Delta \frac{i_j^\Delta}{2} + m_j^\Sigma i_j^\Sigma. \tag{14d}
$$

In Fig. 12 are given diagrams of the all state variables given by differential equations from (14). MMC parameters are chosen as in table x. From diagrams in Fig. 12 can be seen that the first harmonic (angular frequency ω) is dominant in Δ variables, while in Σ variables dominates second harmonic (angular frequency 2ω). In the diagrams per unit values are calculated with the respect to base values: $S_{base} = 1$ GVA, $V_{base} = \frac{V_m}{\sqrt{3}}$ kV
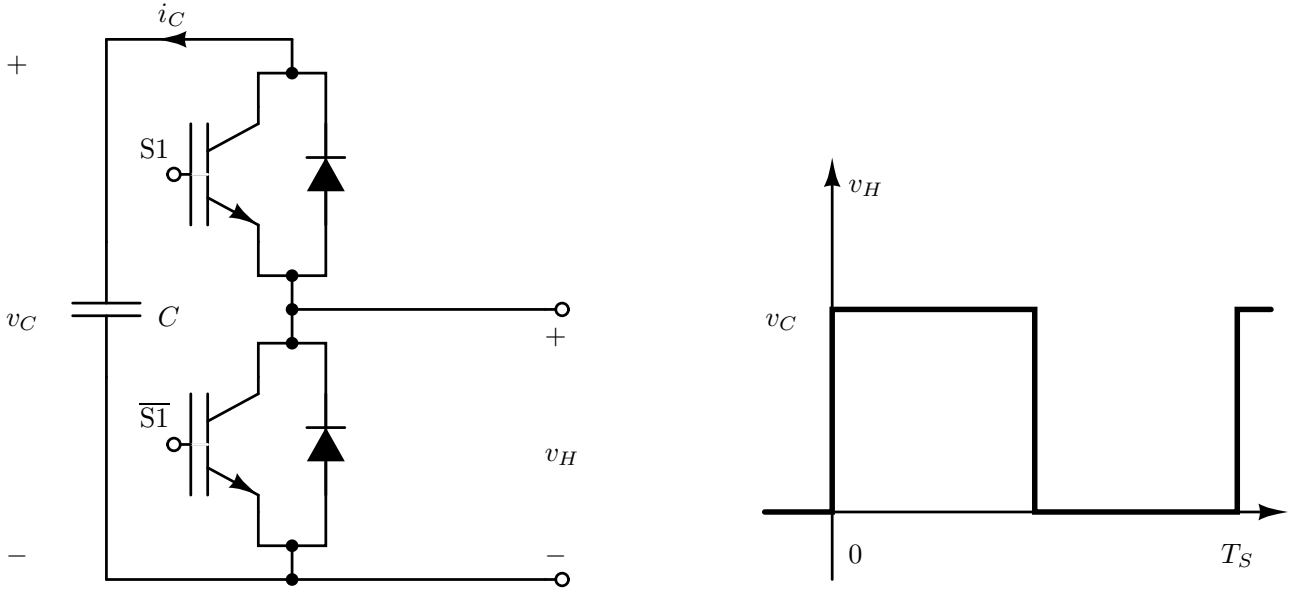
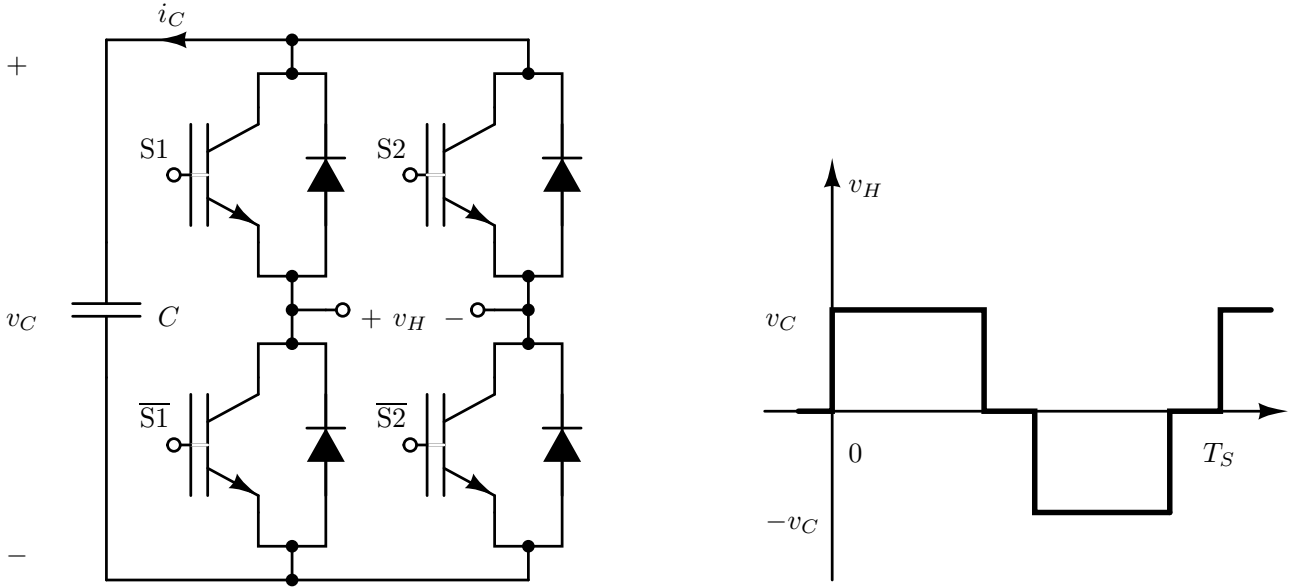Figure 10: HB submodule: left – design; and right – principle of operation.

Figure 11: FB submodule: left – design; and right – principle of operation.

and $I_{base} = \frac{S_{base}}{V_{base}\sqrt{3}}$. Capacitor voltages are represented per unit using DC voltage as base. Modulation indices are set to be $\mathbf{m}_{abc}^{\Sigma} = [1\,1\,1]^T$, and $m_a^{\Delta} = -0.8\cos(\omega t)$, while b and c components are phase shifted by $\frac{2\pi}{3}$ and $\frac{4\pi}{3}$, respectively.

Table 2: MMC parameters

N	400	C_{arm}	$32.55\,\mu\mathrm{F}$	R_{arm}	$1.024\,\Omega$	L_{arm}	48 mH
R_f	$0.521\,\Omega$	L_f	58.7 mH	V_m	320 kV	V_{DC}	640 kV

1.2.3   VSC Control Design

The MMC is controlled using high and low level controls. Control hierarchy is depicted in Fig. 13. Low level controls or inner controlling loops are usually manufactured with the converter itself. They have smaller time constants, usually around 10 ms. High level controls or outer controlling loops can be user configured. Outer controlling loops are used for controlling frequency, energy, power, and DC voltage. They have longer time constants, around 100 ms.
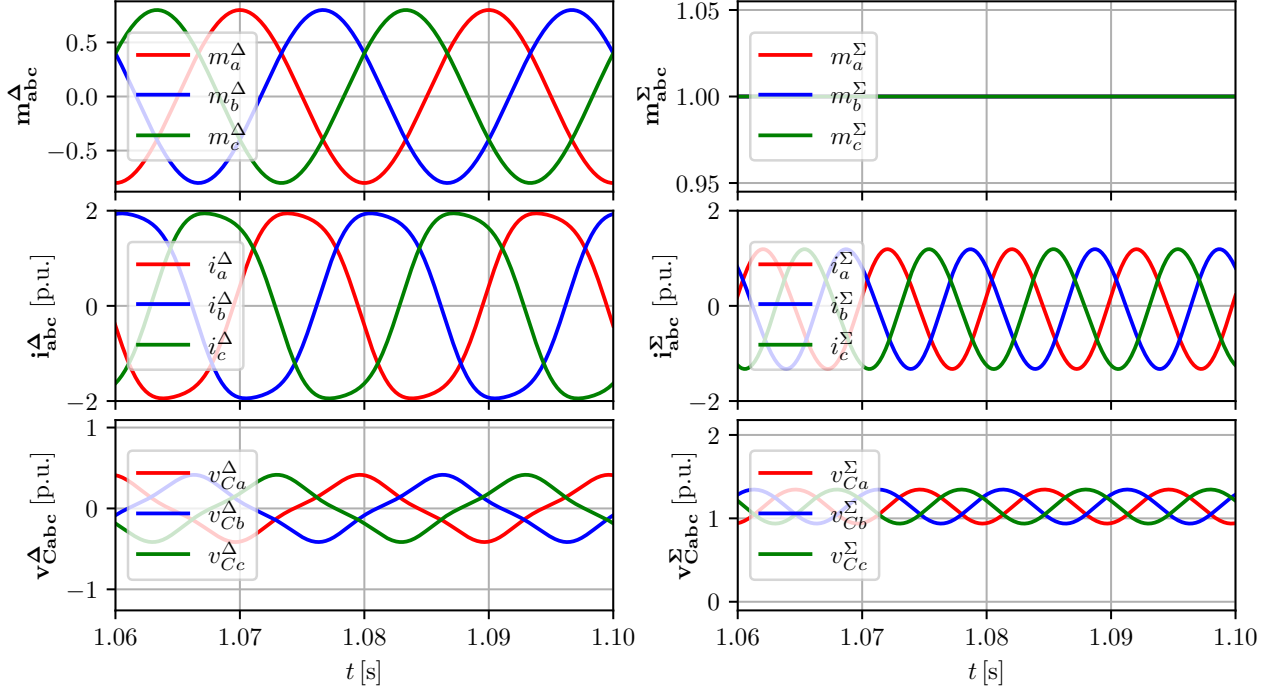
Figure 12: Diagrams of the open-loop MMC.

The most common controls in dqz-frame for an MMC are depicted in Fig. 14. There are presented voltage balancing control for SMs' capacitor voltages, output current control and circulating current control. The SMs' control includes leg voltage control and capacitor voltage balancing control [6]. Since we are considering the MMC with its averaged model, in this course will be not given detailed descriptions about SM control, but they can be found in [6].

1.2.3.1 Inner controlling loops design

Inner controlling loops are capacitor voltage balancing, output current control, circulating current control, and zero current control. In this paragraph we are giving an example how to design output current control and circulating current control.

Output current control can be constructed in abc, $\alpha\beta$ and dq-frames. In this course we will design control using dq-frame formulation. Therefore, we will reformulate equations in abc-frame (14) using Park's transformation on the following matter:

$$\mathbf{T}_{abc\to dq} \times L_{eq}^{ac} \frac{d}{dt} \underbrace{(\mathbf{T}_{dq\to abc} \times \mathbf{i}_{dq}^{\Delta})}_{\mathbf{i}_{abc}^{\Delta}} = L_{eq}^{ac}(\underbrace{\mathbf{T}_{abc\to dq}\dot{\mathbf{T}}_{dq\to abc}}_{\mathbf{J}}\mathbf{i}_{dq}^{\Delta} + \underbrace{\mathbf{T}_{abc\to dq}\mathbf{T}_{dq\to abc}}_{\mathbf{I}}\dot{\mathbf{i}}_{dq}^{\Delta}),$$

where can be calculated that $\mathbf{J}_\omega = \begin{bmatrix} 0 & -\omega \\ \omega & 0 \end{bmatrix}$ and $\mathbf{I}$ is an identity matrix. Therefore, in dq-frame the output current is given as:

$$\dot{\mathbf{i}}_{dq}^{\Delta} = \mathbf{v}_{Mdq}^{\Delta} - \mathbf{v}_{dq}^{G} - (R_{eq}^{ac}\mathbf{I} + L_{eq}^{ac}\mathbf{J}_\omega)\,\mathbf{i}_{dq}^{\Delta}. \tag{15}$$

Similarly, equation for the common circulating current is developed as:

$$\dot{\mathbf{i}}_{dq}^{\Sigma} = \frac{v_{dc}}{2}\begin{bmatrix}1\\1\end{bmatrix} - \mathbf{v}_{Mdq}^{\Sigma} - (R_{arm}\mathbf{I} + L_{arm}\mathbf{J}_{-2\omega})\,\mathbf{i}_{dq}^{\Sigma}. \tag{16}$$

If the controller is defined only using bandwidth ω_n and ζ (instead of K_p and K_i), the proportional and integral gains are tuned using pole-placement method as:

$$\begin{aligned} K_{i,occ} &= L_{eq}^{ac}\,\omega_n^2, \\ K_{p,occ} &= 2\zeta\omega_n L_{eq}^{ac} - R_{eq}^{ac}. \end{aligned}$$

Similarly, the proportional and integral gains of circulating current controller are tuned as:

$$\begin{aligned} K_i &= L_{arm}\,\omega_n^2, \\ K_p &= 2\zeta\omega_n L_{arm} - R_{arm}. \end{aligned}$$
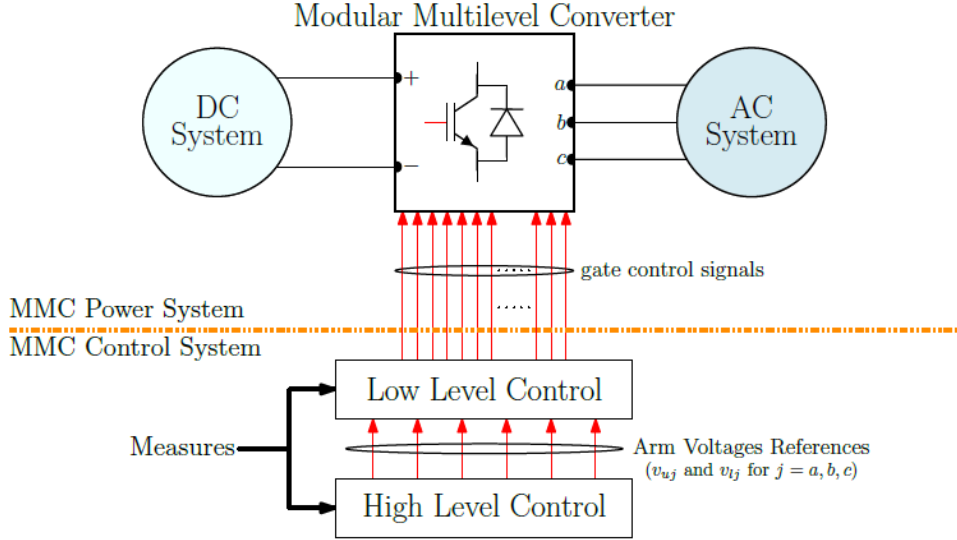
12

Figure 13: MMC control hierarchy, picture taken from [7].

Before we apply these controllers, we have to first transform relevant currents from abc to dq frame. Also, after getting expected voltage references, we have to apply dq to abc transformation on these variables.

1.2.3.2 Outer controlling loops design

Outer controlling loops are power controllers, energy controllers, DC voltage controllers, and frequency controllers.

For HVDC link, power controllers are used on offshore converter side to ensure satisfactory active power transfer. On offshore side is usually used active power controller together with AC voltage controller and PLL (phase locked loop) controller. DC voltage control in PI or droop form is used on onshore side to maintain DC voltage level of the HVDC transmission line. In addition to DC voltage controller, energy controller ensures faster DC voltage and DC current convergence.

Active and reactive power controller design is depicted in Fig. 14, as well as DC voltage PI controller. In addition to DC voltage PI control, DC droop voltage controller is often used. Droop controller is depicted in Fig. 15, which is used to provide active power reference to the converter.
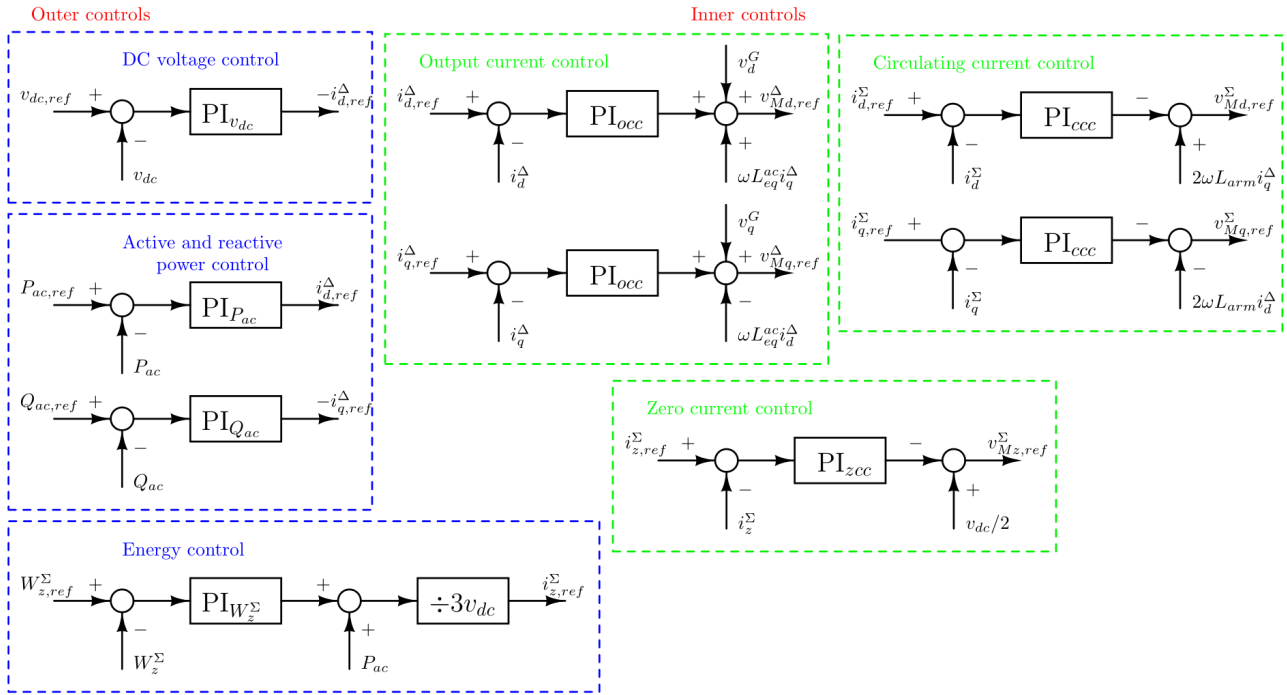
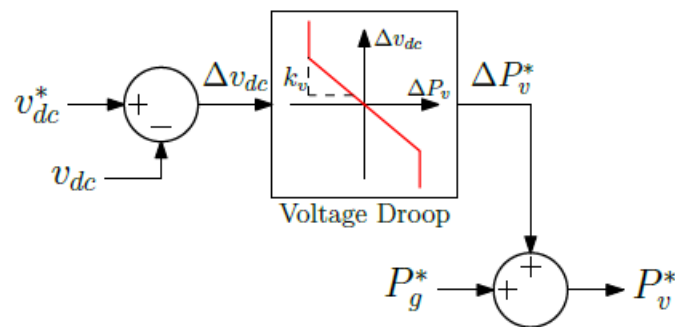Figure 14: Inner and outer controls of the MMC.

Figure 15: MMC DC droop controller, picture taken from [7].

2 MTDC

Multi terminal DC system consists of HVDC transmission system which is through multiple power converters connected to the AC grids. AC grids can be mutually decoupled. As mentioned earlier, in MTDC system power converters are controlled in master-slave manner.

Offshore converters should ensure stable AC voltage of the wind farm, together with stable frequency. For that matter offshore converters have AC voltage controllers, frequency controllers, and PLLs (see Fig. 16) [8]. Offshore converters are denoted to work in islanded mode.
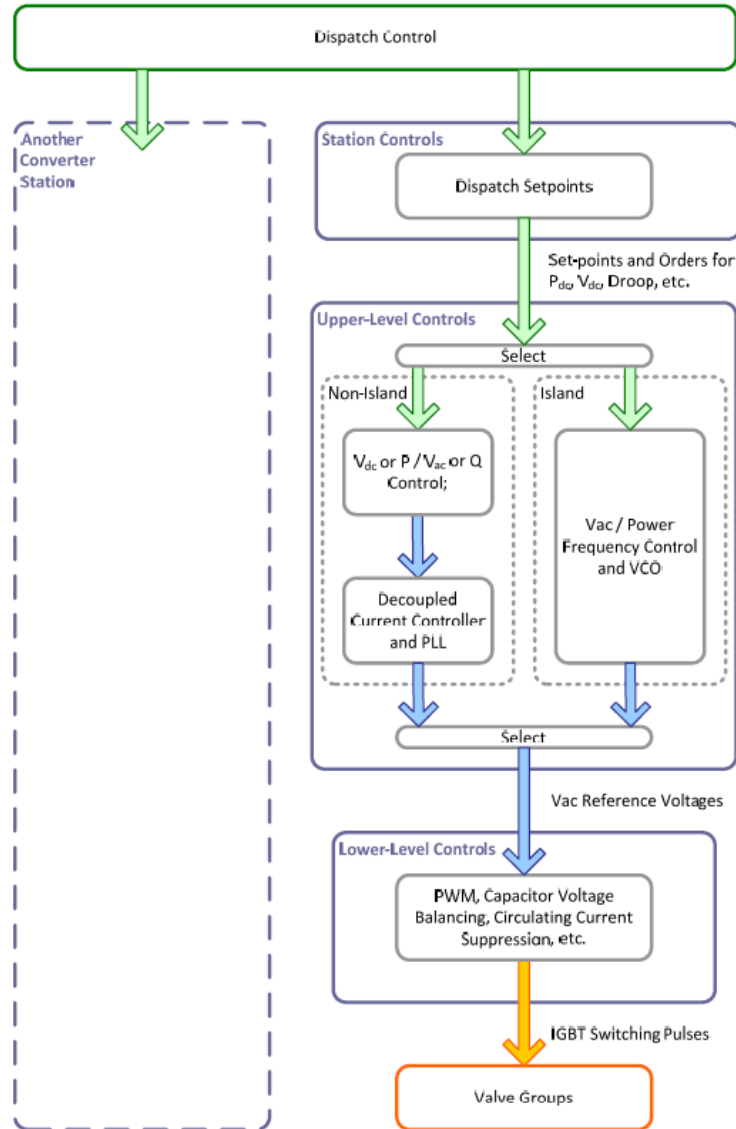

Figure 16: MTDC controls, picture taken from [8].

Onshore power converters should be controlled with two controllers:

1. DC voltage or active power controller;

2. AC voltage or reactive power controller.

Mentioned two controllers produce reference for output current, and zero current.

One example of MTDC is provided in Fig. 17. It can be seen that wind farm connected converters operate in so-called P mode (active power and AC voltage controlled), and that AC grid connected converters operate in V_{dc} droop mode (control of DC voltage and reactive power/AC voltage).
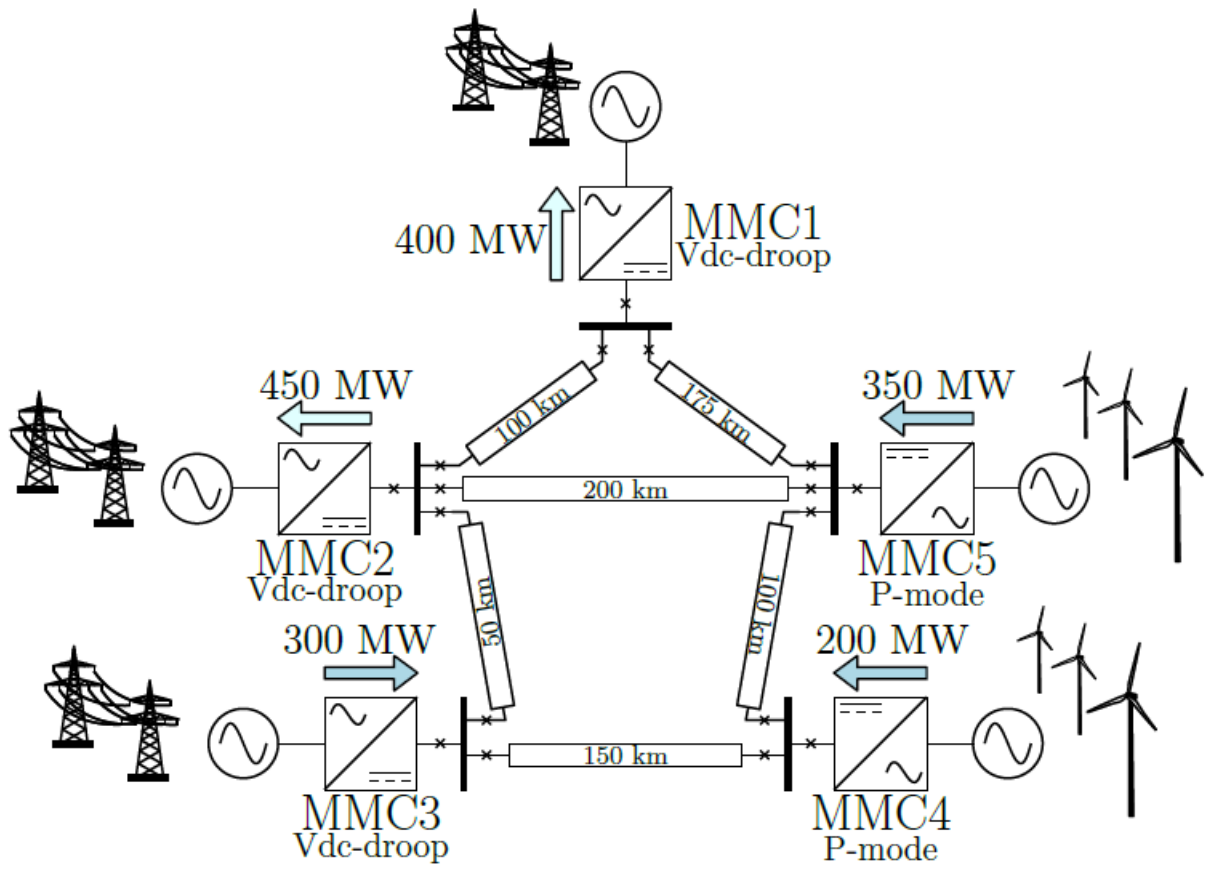
Figure 17: MTDC example, picture taken from [7].

Appendices

A   Transformations

The three-phase system's variables can be represented in the stationary abc-frame, as depicted in Fig. 18. Each vector $\mathbf{f}_{abc}(t)$ is presented as sum of unit vector components f_a, f_b and f_c. It should be noted that the angle of the vector $\mathbf{f}_{abc}$ is time dependent and is given by

$$\theta(t) = \theta_0 + \int_0^t \tau d\tau.$$

The vector $\mathbf{f}_{abc}$ is obtained by projection to a, b and c axis, as:

$$\mathbf{f}_{abc}(t) = \frac{2}{3}\left(\exp(j0)f_a + \exp\left(j\frac{2\pi}{3}\right)f_b + \exp\left(j\frac{4\pi}{3}\right)f_c\right). \tag{17}$$
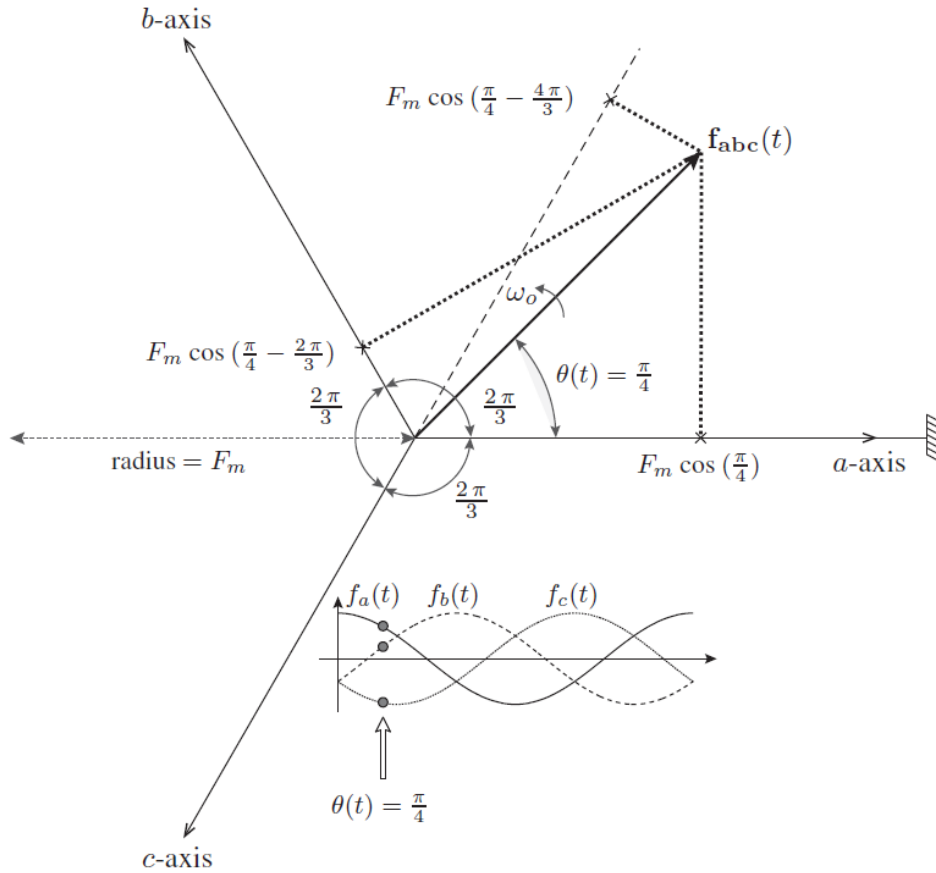

Figure 18: Static abc-frame, picture taken from [6].

Since the phasor in abc-frame is complex in nature and time-varying, the often used frame is $\alpha\beta$-frame depicted in Fig. 19. Vector in this frame is represented by two components, α and β, obtained by projecting vector on the two orthogonal axes. Vector's value is then:

$$\mathbf{f}_{\alpha\beta}(t) = f_\alpha(t) + jf_\beta(t). \tag{18}$$

The transformation from abc-frame to $\alpha\beta$-frame is obtained by applying Clarke's transformation:

$$\begin{bmatrix} f_\alpha(t) \\ f_\beta(t) \end{bmatrix} = \underbrace{\begin{bmatrix} 1 & -\frac{1}{2} & -\frac{1}{2} \\ 0 & \frac{\sqrt{3}}{2} & -\frac{\sqrt{3}}{2} \end{bmatrix}}_{\mathbf{T}_{abc\rightarrow\alpha\beta}} \times \begin{bmatrix} f_a(t) \\ f_b(t) \\ f_c(t) \end{bmatrix}, \tag{19}$$

17

while the inverse Clarke's transformation is:

$$\begin{bmatrix} f_a(t) \\ f_b(t) \\ f_c(t) \end{bmatrix} = \underbrace{\begin{bmatrix} 1 & 0 \\ -\frac{1}{2} & \frac{\sqrt{3}}{2} \\ -\frac{1}{2} & -\frac{\sqrt{3}}{2} \end{bmatrix}}_{\mathbf{T}_{\alpha\beta \to abc}} \times \begin{bmatrix} f_\alpha(t) \\ f_\beta(t) \end{bmatrix}. \tag{20}$$
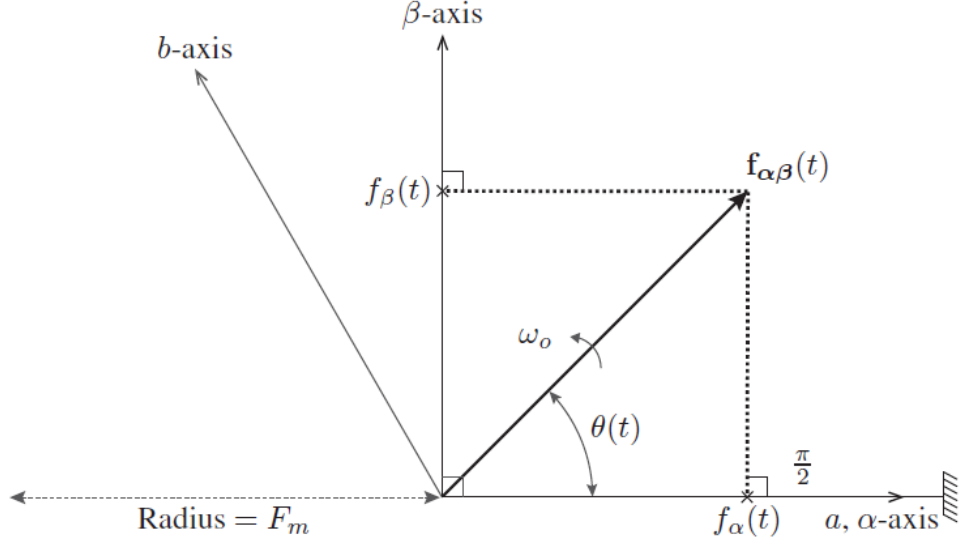

Figure 19: Static $\alpha\beta$-frame, picture taken from [6].

Further more, the power system is often modeled in the rotating dq-frame. This frame is two axes frame rotating with the synchronous frequency, depicted in Fig. 20. The space phasor is given by:

$$\mathbf{f}_{dq}(t) = f_d(t) + j f_q(t),$$

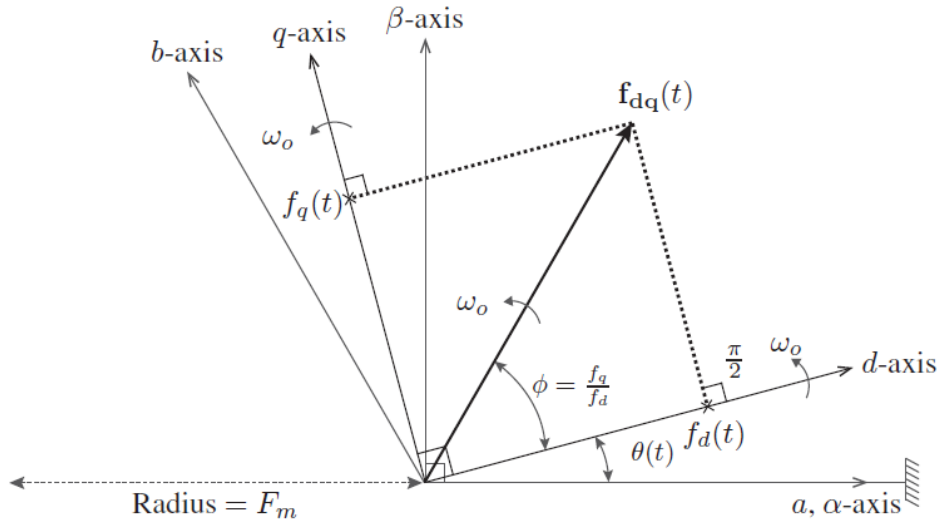where the space phasor has the static position θ towards the axes.

Figure 20: Rotating dq-frame, picture taken from [6].

The complete AC power system is modeled in dqz-frame to fit the developed power converter model. For that purpose, it was necessary to apply abc to dqz transformation.

In order to transform three-phase voltages and currents from the stationary abc-frame to the rotating dqz-

frame, Park's transformation defined as

$$\begin{bmatrix} f_d(t) \\ f_q(t) \end{bmatrix} = \frac{2}{3} \underbrace{\begin{bmatrix} \cos(\omega_0 t) & \cos\left(\omega_0 t - \frac{2\pi}{3}\right) & \cos\left(\omega_0 t - \frac{4\pi}{3}\right) \\ -\sin(\omega_0 t) & -\sin\left(\omega_0 t - \frac{2\pi}{3}\right) & -\sin\left(\omega_0 t - \frac{4\pi}{3}\right) \end{bmatrix}}_{\mathbf{T}_{abc \to dq}} \times \begin{bmatrix} f_a(t) \\ f_b(t) \\ f_c(t) \end{bmatrix}, \tag{21}$$

is employed. The inverse Park's transformation is given as

$$\begin{bmatrix} f_a(t) \\ f_b(t) \\ f_c(t) \end{bmatrix} = \underbrace{\begin{bmatrix} \cos(\omega t) & -\sin(\omega t) \\ \cos\left(\omega_0 t - \frac{2\pi}{3}\right) & -\sin\left(\omega_0 t - \frac{2\pi}{3}\right) \\ \cos\left(\omega_0 t - \frac{4\pi}{3}\right) & -\sin\left(\omega_0 t - \frac{4\pi}{3}\right) \end{bmatrix}}_{\mathbf{T}_{dq \to abc}} \times \begin{bmatrix} f_d(t) \\ f_q(t) \end{bmatrix}. \tag{22}$$

B Setting up Python

There are several ways for Python installation on Windows. Standard installation ensures running of the Python code from the Windows console. Anaconda offers a nice GUI for Python named Spyder and enables installation of the packages online. The newest individual edition of Anaconda can be found on link `https://www.anaconda.com/products/individual`, and it contains Python version 3.8.5. New Python packages can be installed inside Anaconda Prompt in administrator mode by running command `conda install -c conda-forge pkg_name` if the package is available in Anaconda repositories. Otherwise, command `python -m pip install pkg_name` is used for known packages inside Python repositories or `python -m pip install git+git_location` for packages on Github.

Python can be started by opening Spyder. Spyder interface is shown in Fig. 21. It offers script view on the left side and an interactive console on the right side.
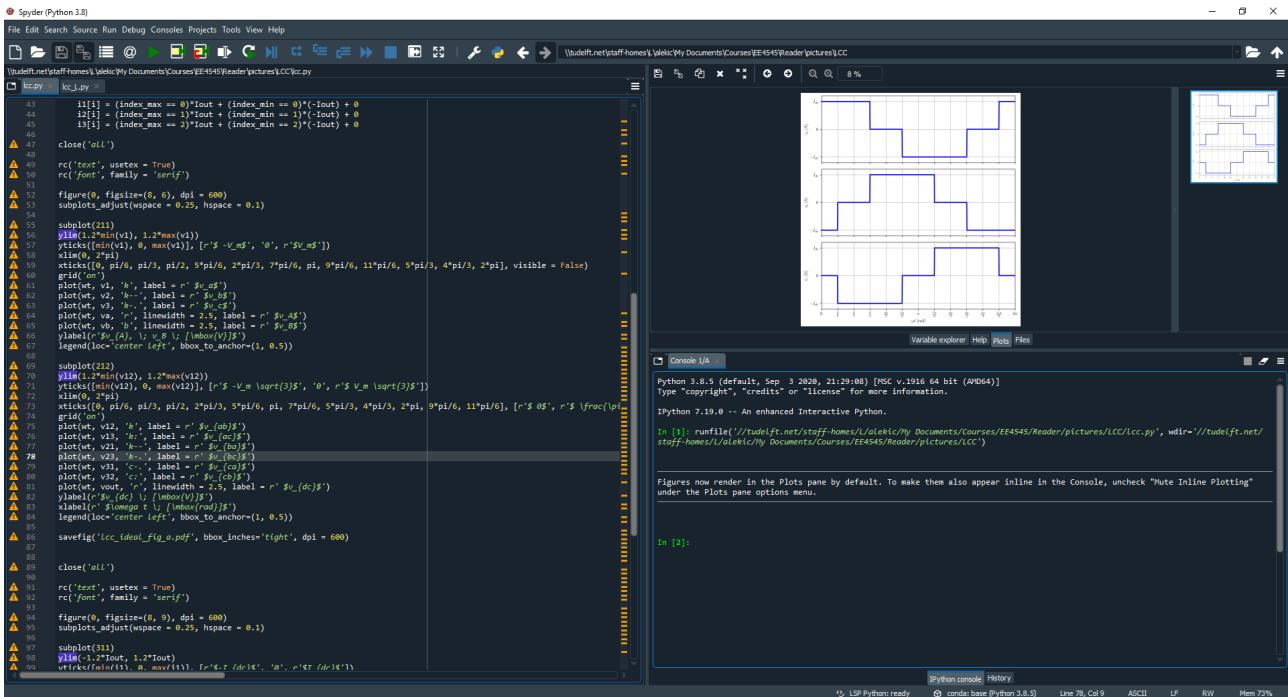

Figure 21: Spyder interface.

For this course the following packages should be installed in `Anaconda prompt` running it as administrator:

- Matplotlib - command: `conda install -c conda-forge matplotlib`.

Since course codes have LaTeX visualisations, there should be LaTeX compiler installed on the computer. The compiler we will be using is Miktex (`https://miktex.org/download`). **While installing it, the option for automatic package installation should be selected.**

References

[1] M. Ramamoorty, *An Introduction to thyristors and their applications.* Macmillan International Higher Education, 1978.

[2] M. Daryabak, "Modeling line-commutated converter hvdc transmission systems using dynamic phasors," Ph.D. dissertation, University of Manitoba, 2014.

[3] M. Daryabak, S. Filizadeh, J. Jatskevich, A. Davoudi, M. Saeedifard, V. Sood, J. Martinez, D. Aliprantis, J. Cano, and A. Mehrizi-Sani, "Modeling of lcc-hvdc systems using dynamic phasors," *IEEE Transactions on Power Delivery*, vol. 29, no. 4, pp. 1989–1998, 2014.

[4] W. Hammer, "Dynamic modeling of line and capacitor commutated converters for hvdc power transmission," Ph.D. dissertation, ETH Zurich, 2003.

[5] O. Anaya-Lara, D. Campos-Gaona, E. Moreno-Goytia, and G. Adam, *Offshore wind energy generation: control, protection, and integration to electrical systems.* John Wiley & Sons, 2014.

[6] S. Du, A. Dekka, B. Wu, and N. Zargari, *Modular multilevel converters: analysis, control, and applications.* John Wiley & Sons, 2017.

[7] S. Akkari, "Control of a multi-terminal hvdc (mtdc) system and study of the interactions between the mtdc and the ac grids." Ph.D. dissertation, Université Paris-Saclay, 2016.

[8] T. K. Vrana, Y. Yang, D. Jovcic, S. Dennetière, J. Jardini, and H. Saad, "The cigre b4 dc grid test system," *Electra*, vol. 270, no. 1, pp. 10–19, 2013.